Reservoir characterization using perforation shots: anisotropy and attenuation

Zhishuai Zhang[1], Jing Du[2], and Gary M. Mavko[1]*
[1]Stanford University, [2]Total E&P Research and Technology, LLC

Summary

Anisotropic parameters, even if considered in a microseismic processing, are typically simultaneously inverted with microseismic event locations. This usually leads to an under-constrained inverse problem that highly dependent on prior/initial information. In this paper, we carefully processed the waveforms from perforation shots so that SV-wave arrival times can be picked in addition to P- and SH-wave arrival times. This makes the inversion well-constrained by reducing the number of model parameters while increasing the number of observations. We applied both Maximum A posteriori (MAP) estimation and Randomized Maximum Likelihood (RML) method for anisotropic parameter estimation and uncertainty quantification. Results verified the stableness of the inversion and revealed the uncertainty and tradeoffs among model parameter. On the other hand, attenuation is generally not considered in microseismic modeling and processing. Our study found that hydraulic stimulation can lead severe seismic attenuation to reservoirs. The attenuation can dramatically change waveform characters and causes velocity dispersion. Thus, sonic logs, which are acquired at frequencies much higher than seismic data frequency should not be used directly for data processing in hydraulic stimulated zones.

Introduction

In microseismic processing, perforation shots have been routinely used for isotropic velocity model calibration. However, shales, especially organic rich shales, are almost always anisotropic (Vernik, 2016). A reliable estimation of anisotropic parameters at reservoir in-situ condition not only improves microseismic event location accuracy but also be essential for reservoir characterization and providing information for active source surface seismic survey (Du et al., 2013; Vernik and Nur, 1992). Research on anisotropic earth model characterization has been carried out but mainly on simultaneous inversion of microseismic event locations and anisotropic parameters (Grechka et al., 2011; Li et al., 2013; Yuan and Li, 2017). In this study, we were able to determine the arrival times of SV-waves, in addition to the traditionally used P- and SH-waves, with high confidence. Using perforation shots instead of microseismic events avoids the trade-offs between source locations and velocity parameters (Zhang et al., 2017), do not need to be inverted. These efforts result in a relatively well-constraint inverse problem that is insensitive to the prior model. We use both deterministic and stochastic approaches to investigate the uncertainties in anisotropic velocity model estimation. Results show the stableness of the inversion and help to understand the uncertainty and tradeoffs between model parameters.

The importance of estimating Q value lies in several aspects. Firstly, the seismic attenuation acts as a low pass filter that manipulate the frequency content of seismic waves. Thus, it is a requirement for understanding and making any use of the full waveform information. Secondly, the Q value can be a parameter to help understand the in-situ conditions of the target formation. Finally, attenuation relates to velocity dispersion (Toll, 1956). The determination of Q value can be from surface reflection seismology, crosswell (Quan and Harris, 1997), or Vertical Seismic Profile (VSP) data (Tonn, 1991). There are only a limited number of studies to investigate the Q values changes due to fluid injection. Here, we use the spectral ratio method to estimate Q values with perforation shot data (Tonn, 1991). The estimated stage-dependent attenuation reveals the possible effect introduced by hydraulic stimulation. It also suggests that downhole seismic survey could be a suitable tool to monitor this process.

Hydraulic fracturing project overview

The hydraulic fracturing stimulation was conducted with a horizontal well in the Vaca Muerta Formation at Neuquén, Argentina. The Vaca Muerta Formation consists of three members. The lower Vaca Muerta is organic-rich shale. The middle Vaca Muerta shows less lamination and lower TOC content. The upper Vaca Muerta is also more organic rich and laminated like the lower member (Garcia et al., 2013). The overlying Quintuco formation is primarily a limestone reservoir with dolomite and anhydrite. The underlying Tordillo is a clastic reservoir deposited through eolian and lacustrine mechanisms (Willis et al., 2014).

The side view and map view of the project is shown in Figure 1. The stimulation well is perpendicular to the expected fracture azimuth in the Vaca Muerta. It is completed as a cemented lateral using a plug-and-perf. A total of eight hydraulic fracturing treatment stages were performed. Each stimulation stage follows four perforation shots. The stimulation process was monitored with an array of eleven geophones in a nearby vertical well. The geophones and perforation shots are almost in the same vertical plane. The vertical spacing is approximately 30.5 m for the top four geophones and is approximately 15.2 m for the bottom eight geophones. The sampling interval of the recording is 0.375 ms.

10.1190/segam2018-2997629.1

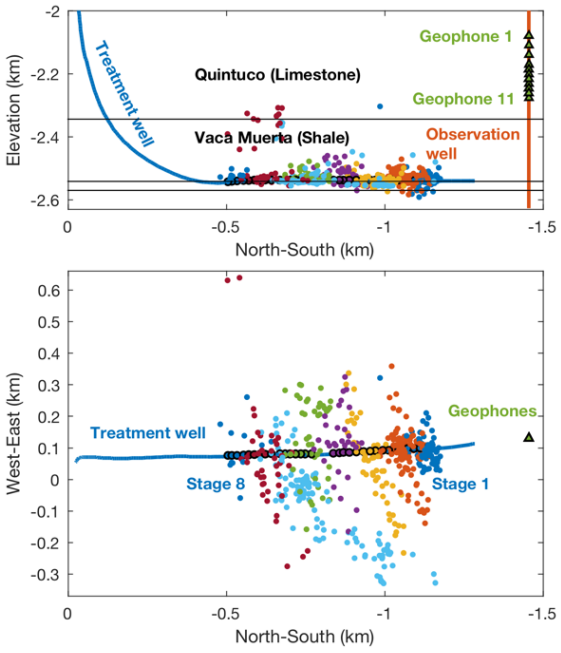

Figure 1: Microseismic survey project setup. The microseismic events are color coded according to their stages.

Anisotropy

A sample waveforms from the first perforation in stimulation Stage 2 is shown in Figure 2. They are rotated based on P-wave polarization to separate P-, SH-, and SV-wave components. The phase annotated by the red arrow in the P-wave panel is tube wave as discussed in our previous study (Bergery *et al.*, 2017). We can see clear shear wave splitting as indicated by the manually picked SH- and SV-wave arrival times. This is an effect of anisotropy and indicate the necessity to take it into consideration. To characterize the anisotropic earth model, we divided the studied area into four horizontal layers based on well logs and sensitivities to arrival times. The initial model is a homogeneous isotropic model.

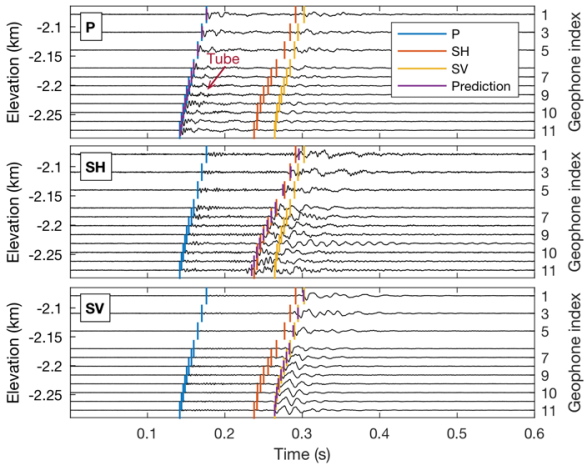

Figure 2: Sample waveforms from the first perforation in stimulation Stage 2. Waveforms are rotated to separate P-, SH-, and SV-waves.

The observations are manually picked arrival times of P-, SH-, and SV-waves. We picked P- and SH-waves for all perforations shots whenever we were able to do so confidently. The SV-wave arrival times for the twelve perforation shots in the first three stimulation stages were also picked.

We used a Randomized Maximum Likelihood (RML) method (Oliver et al., 1996) and the Maximum A Posterior (MAP) estimation (Tarantola, 2005) to solve the inverse problem stochastically and deterministically.

First, we generated 50 realizations from the posterior probability density function with the RML method. Then, the histogram of each variable was fitted with a kernel smoother and the result is shown in Figure 3. The overlain orange lines represent the MAP estimation results for comparison purpose. In general, the RML result matches the

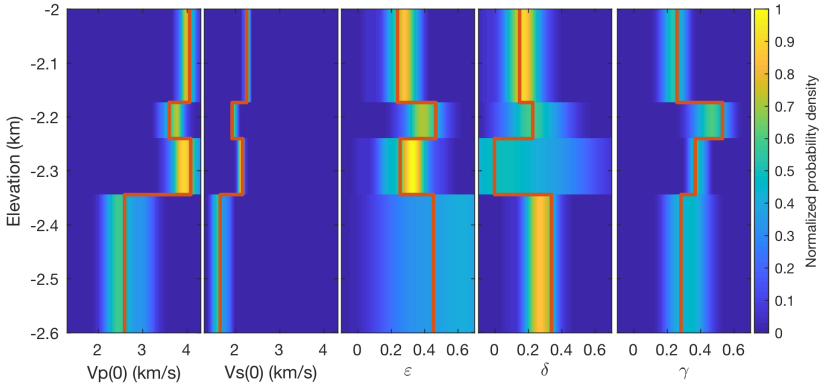

Figure 3: RML estimated probability density overlain by the MAP estimated result (orange lines). The estimation uncertainty at the bottom layer is large due to lack of sensitivity to arrival times.

10.1190/segam2018-2997629.1

MAP estimation relatively well. From the RML result, we can see increased velocity estimation uncertainty with depth.

The MAP model estimated is shown in Figure 4 along with the sonic logs and gamma ray log. The estimated vertical propagated P- and S-waves match the sonic log relatively well for the top three layers. However, those for the bottom layer is significantly smaller than the sonic logs. This discrepancy might be a result a velocity dispersion related to severe attenuation as will be discussed in the next section.

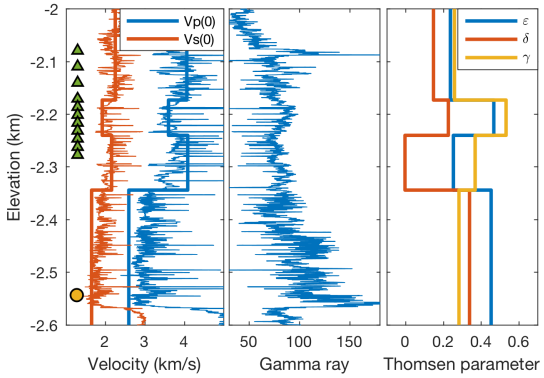

Figure 4: MAP estimated velocity model with well logs as the background.

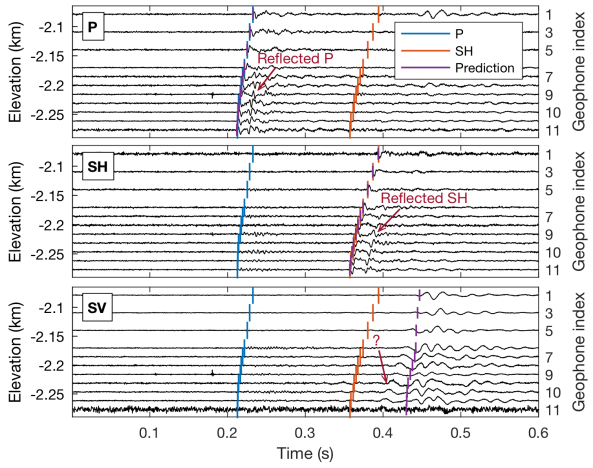

Figure 5: Waveform from the second perforation in Stage 6 stimulation. Even though SV-wave arrival times are not used in velocity model estimation, the predictions given by the estimated model match the waveform well. The unknown phase annotated by the question mark may be misidentified as SV-wave otherwise.

The predicted arrival times using the inverted model is shown by the purple lines in Figure 2 (Stage 2, Perforation 1) and Figure 5 (Stage 6, Perforation 2). Only SV-wave arrival times from Stage 1 to Stage 3 are used for inversion, so those in later stages can be used to validate the inverted model. The predicted SV-wave arrival times in Figure 5 match well with the waveforms. Also note the phase indicated by the red question mark in the SV-wave component panel, which might be P-SV converted waves. This phase can be misinterpreted as the direct SV-wave without the prediction from the inverted model.

Attenuation

A zoom in view of the P-wave component from Figure 2 is shown in Figure 6 (a). We can see clear change in frequency content from the top to the bottom geophone. We attribute this change is to attenuation along the paths of the seismic waves. With the spectral-ratio method, we may estimate the Q values along each path. Due to limitation in signal to noise ratio (S/N) and ray path coverage, we assumed an isotropic and homogeneous Q model within the studied area. This represents the average Q values along the seismic paths. An example spectral-ratio fit is shown in Figure 6 (b). The estimated Qp value from this spectrum is 11.5, which means significant attenuation within the area.

We calculate the Qp values using perforation shot signals with the spectral-ratio method (Tonn, 1991). To achieve a reliable estimation result, we only used perforation shots that can give a reasonable linear relationship between spectral ratio and frequency. Figure 7 shows the estimated Q values with their perforation shot locations. It is apparent that the perforation shots with high Q values are all from Stage 1, which is the only stage that no hydraulic fracturing stimulation was conducted before the perforation. Thus, we consider these Q values represent the original attenuation of the unstimulated reservoir. After Stage 1, the ray paths of the perforation shots will somewhat overlap with the zones affected by previous stimulations. The significant decrease in the Q values estimated from later-stages perforation shots may be related to the stimulation of the formation.

We see discrepancy between estimated velocities and the sonic logs at the bottom layer in Figure 4. One possible explanation to this discrepancy between the MAP estimated model and the well log at the bottom layer is a result of velocity dispersion. Since we have observed severe attenuation within the studies area, causality requires corresponding velocity dispersion in this area (Toll, 1956). Thus, the sonic log may not be a good representation of the wave velocity at the microseismic frequency range. Here, we used a nearly constant Q model to relate the discrepancy between the MAP estimated velocity and the sonic log at the bottom layer (Liu et al., 1976; Mavko et al., 2009). According to the nearly constant Q model,

$$\frac{V(\omega)}{V(\omega_0)} = 1 + \frac{1}{\pi Q}\ln\left(\frac{\omega}{\omega_0}\right), \qquad (1)$$

10.1190/segam2018-2997629.1

where $V(\omega)$ and $V(\omega_0)$ are velocities at two different frequencies ω and ω_0 within the band where Q is nearly constant.

Assuming the pickings of the arrival times represent a frequency of $\omega_0 = 200\ Hz$ and the sonic log was acquired at a frequency of $\omega = 20\ kHz$, the left-hand side (LHS) of equation (1) is

$$LHS = \frac{Vp(\omega)}{Vp(\omega_0)} = \frac{Vp(20\ kHz)}{Vp(200\ Hz)} \approx \frac{3.0\ km/s}{2.6\ km/s} \approx 1 + 0.15. \quad (2)$$

Using a Qp value of 13 from our estimation, the right-hand side (RHS) of equation (1) is

$$RHS = 1 + \frac{1}{\pi Qp} \ln\left(\frac{\omega}{\omega_0}\right) \approx 1 + 0.11. \quad (3)$$

The LHS is approximately equal to the RHS of equation (1) based on this analysis. This shows the attenuation at least partially explain the discrepancy between the estimated result and the sonic log result at the bottom layer.

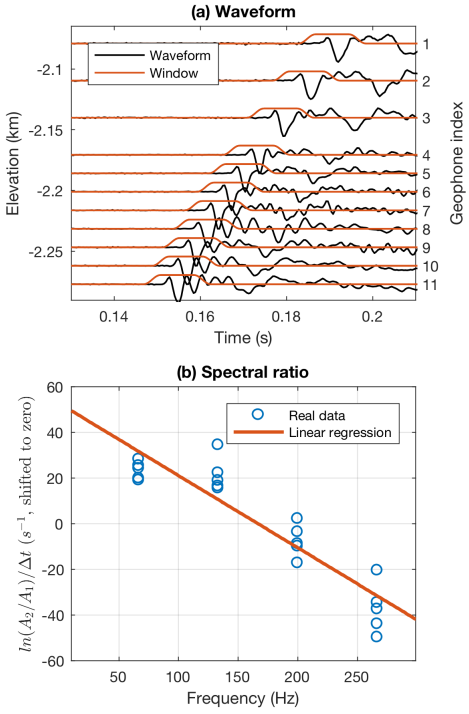

Figure 6: (a) Zoom-in view of the P-wave component of the waveform in Fig. 2. Comparing the waveforms from different geophones using the orange windows as reference, the frequency content at the top traces are significantly lower than those at the bottom traces. This is an indication of severe attenuation. (b) spectral ratio of the waveform in (a).

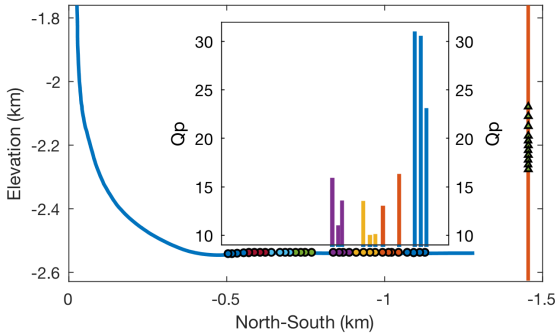

Figure 7: Estimated Qp values using perforation shots by stage.

Conclusions

With little requirement of sonic logs as the prior information, we were able to build an anisotropic earth model using only microseismic data. RML estimation verify the stableness of the inversion and help understanding the uncertainties and tradeoffs among velocity model parameters. The inverted vertically propagated Vp and Vs match well with sonic log data in area that are unaffected by hydraulic stimulation. Our work also shows the hydraulic stimulation process will cause significantly attenuation to seismic waves. Causality requires a corresponding velocity dispersion associated with attenuation. Thus, traditional processing practice of using sonic logs, which are acquired at frequencies much higher than microseismic data frequency, may be questionable. It also shows the possibility to monitor hydraulic stimulation with attenuation analysis.

Acknowledgements

The authors would like to thank Total S. A., Total Austral and its partners for granting permission to publish this paper.

10.1190/segam2018-2997629.1

REFERENCES

Du, J., N. Warpinski, and C. Waltman, 2013, Anisotropic effects on polarization from highly deviated / horizontal wells in microseismic monitoring of hydraulic fractures: 83th Annual International Meeting, SEG, Expanded Abstracts, 2008–2012, https://doi.org/10.1190/segam2013-0215.1.

Garcia, M. N., F. Sorenson, J. C. Bonapace, F. Motta, C. Bajuk, and H. Stockman, 2013, Vaca Muerta Shale Reservoir characterization and description: the starting point for development of a shale play with very good possibilities for a successful project: Paper presented at Unconventional Resources Technology Conference, URTEC 1508336-MS, https://doi.org/10.1190/urtec2013-090.

Grechka, V., P. Singh, and I. Das, 2011, Estimation of effective anisotropy simultaneously with locations of microseismic events: Geophysics, **76**, no. 6, WC143–WC155, https://doi.org/10.1190/geo2010-0409.1.

Li, J., H. Zhang, W. L. Rodi, and M. N. Toksoz, 2013, Joint microseismic location and anisotropic tomography using differential arrival times and differential backazimuths: Geophysical Journal International, **195**, 1917–1931, https://doi.org/10.1093/gji/ggt358.

Liu, H.-P., D. L. Anderson, and H. Kanamori, 1976, Velocity dispersion due to anelasticity: Implications for seismology and mantle composition: Geophysical Journal International, **47**, 41–58, https://doi.org/10.1111/j.1365-246X.1976.tb01261.x.

Mavko, G., T. Mukerji, and J. Dvorkin, 2009, The rock physics handbook: Tools for seismic analysis of porous media: Cambridge University Press.

Oliver, D. S., N. He, and A. C. Reynolds, 1996, Conditioning permeability fields to pressure data: Paper presented at ECMOR V-5th European Conference on the Mathematics of Oil Recovery, https://doi.org/10.3997/2214-4609.201406884.

Quan, Y., and J. M. Harris, 1997, Seismic attenuation tomography using the frequency shift method: Geophysics, **62**, 895–905.

Tarantola, A., 2005, Inverse problem theory and methods for model parameter estimation: Society for Industrial and Applied Mathematics (SIAM).

Toll, J. S., 1956, Causality and the dispersion relation: Logical foundations: Physical Review, **104**, 1760–1770, https://doi.org/10.1103/PhysRev.104.1760.

Tonn, R., 1991, The determination of the seismic quality factor Q from VSP data: A comparison of different computational methods: Geophysical Prospecting, **39**, 1–27, https://doi.org/10.1111/j.1365-2478.1991.tb00298.x.

Vernik, L., 2016, Seismic petrophysics in quantitative interpretation: Society of Exploration Geophysicists.

Vernik, L., and A. Nur, 1992, Ultrasonic velocity and anisotropy of hydrocarbon source rocks: Geophysics, **57**, 727–735, https://doi.org/10.1190/1.1443286.

Willis, M., A. N. Tutuncu, and A. Padin, 2014, Integration of core data with well logs for geomechanical property determination and monitoring in the Argentinean Vaca Muerta Shale Formation: Paper presented at Unconventional Resources Technology Conference, URTEC 1922481-MS, https://doi.org/10.15530/urtec-2014-1922481.

Yuan, D., and A. Li, 2017, Joint inversion for effective anisotropic velocity model and event locations using S-wave splitting measurements from downhole microseismic data: Geophysics, **82**, no. 3, C133–C143, https://doi.org/10.1190/geo2016-0221.1.

Zhang, Z., J. W. Rector, and M. J. Nava, 2017, Simultaneous inversion of multiple microseismic data for event locations and velocity model with Bayesian inference: Geophysics, **82**, no. 3, KS27–KS39, https://doi.org/10.1190/geo2016-0158.1.